

FACULTY OF ENGINEERING LTH AT LUND  
UNIVERSITY

MASTER THESIS

---

**Structural Effects on Degradation and  
Photophysical Behaviour of  
Methylammonium Lead Iodide  
Perovskites**

---

*Author:*  
Elin KÄLLMAN

*Supervisor:*  
Ivan SCHEBLYKIN  
Aboma MERDASA

*A thesis submitted in fulfillment of the requirements  
for the degree of Master of Science, Degree programme in Engineering  
Physics*

*of the*

Department of Chemical Physics

October 27, 2016



FACULTY OF ENGINEERING LTH AT LUND UNIVERSITY

## *Abstract*

Department of Chemical Physics

Master of Science, Degree programme in Engineering Physics

### **Structural Effects on Degradation and Photophysical Behaviour of Methylammonium Lead Iodide Perovskites**

by Elin KÄLLMAN

Perovskites have proven to have very promising properties applicable in future higher efficient technological devices such as light emitters and solar cells. In further development of perovskite solar cell devices there are however serious material drawbacks such as instability and toxicity, causing the perovskite research community to question if and how these obstacles can be overcome.

In this work, the structure dependent photoluminescent (PL) properties of perovskites have been investigated through correlation of fluorescence microscopy and electron microscopy. We encountered structural differences in degradation of bulk samples along with variations of PL intensity and PL lifetime between different structures. Structural inhomogeneity was proven to have a big impact on non-radiative decay of perovskite structures with sizes of a few mikrons.



# Contents

<b>Abstract</b>	<b>iii</b>
<b>1 Introduction to the thesis topic</b>	<b>1</b>
<b>2 Background information and theory</b>	<b>3</b>
2.1 Semiconductor Fundamentals . . . . .	3
2.2 Perovskites Properties . . . . .	4
<b>3 Experimental setup</b>	<b>7</b>
3.1 Synthesis . . . . .	7
3.1.1 Method 1 . . . . .	7
3.1.2 Method 2 . . . . .	8
3.2 Instrumental Description . . . . .	8
3.2.1 PL-measurement Setup . . . . .	8
CCD-measurements . . . . .	9
Method of Reaching Super Resolution . . . . .	9
Time-Correlated Single Photon Counting (TCSPC) . . . . .	10
3.2.2 Scanning Electron Microscope . . . . .	11
<b>4 Results of Different Synthesis</b>	<b>13</b>
<b>5 Degradation of Bulk Samples</b>	<b>15</b>
5.1 Photoinduced Degradation Process . . . . .	15
5.2 Experimental Description . . . . .	15
5.2.1 Spectral difference . . . . .	16
5.2.2 Structural Difference . . . . .	16
5.3 Atmospheric dependence: Air and N <sub>2</sub> . . . . .	17
5.4 Degradation at Higher Power . . . . .	17
5.4.1 Structural difference . . . . .	18
5.4.2 Surviving Intensity Oscillating Area . . . . .	18
<b>6 Life-time Measurements of MAIPbI<sub>3</sub></b>	<b>23</b>
6.1 Background of Luminescent Lifetime . . . . .	23
6.2 Structural dependence of lifetime . . . . .	23
6.3 Blinking Structures . . . . .	25
<b>7 Discussion of the Experimental Results</b>	<b>27</b>
7.1 Synthesis . . . . .	27
7.2 Degradation of Bulk Samples . . . . .	27
7.2.1 Degradation at Higher Power . . . . .	28
7.2.2 Oscillating Intensity . . . . .	28
7.2.3 Blinking Causing Change of Emissive Point . . . . .	28
7.3 Luminescent Life-Time of Different Structures . . . . .	29
7.3.1 Blinking and Lifetime . . . . .	30

<b>8 Conclusion and future directions</b>	<b>31</b>
<b>A Equi-molar MAIPbI<sub>3</sub> Perovskite Preparation Instruction</b>	<b>33</b>
A.1 M1 . . . . .	33
A.1.1 PbI <sub>2</sub> + MAI (461 mg + 159 mg, 1:1 molar ratio) to pre- pare 0.8 M solution of MAPbI <sub>3</sub> . . . . .	33
A.2 M2 . . . . .	33
A.2.1 MAPbI <sub>3</sub> nano-wire preparation . . . . .	33
<b>References</b>	<b>35</b>

# List of Figures

2.1	Basics of traps in semiconductor systems. . . . .	3
2.2	Perovskite crystal structure. . . . .	5
3.1	Experimental setup for PL measurements. . . . .	8
3.2	Basic function of TCSPC. . . . .	11
4.1	A comparison of structural results of different synthesizing methods. . . . .	13
5.1	Structural deformation of MAPbI <sub>3</sub> to PbI <sub>2</sub> under photoinduced degradation. . . . .	15
5.2	Florescent spectrum with additional information. . . . .	16
5.3	Results from the degradation experiment in air. . . . .	17
5.4	Degradation in air and N <sub>2</sub> . . . . .	18
5.5	Overview SEM image of the high-power-degraded line. . . . .	19
5.6	Results from surviving structure in degraded area captured by CCD. . . . .	20
5.7	Blinking connected to variation of emissive point for a crystal. . . . .	21
6.1	Luminescent lifetimes associated with crystal structures. . . . .	24
6.2	Blinking vs. luminescent lifetime. . . . .	25





# List of Abbreviations

<b>PL</b>	<b>PhotoLuminescence</b>
<b>M1</b>	<b>Method 1</b>
<b>M2</b>	<b>Method 2</b>
<b>VB</b>	<b>Valence Band</b>
<b>CB</b>	<b>Conduction Band</b>
<b>VBM</b>	<b>Valence Band Maximum</b>
<b>CBM</b>	<b>Conduction Band Minimum</b>



# Physical Constants

Boltzmann Constant  $k = 1.380\,648\,52 \times 10^{-23} \text{ kg m}^2 \text{ s}^{-2} \text{ K}^{-1}$

Planck's Constant  $h = 6.626\,070\,04 \times 10^{-34} \text{ kg m}^2 \text{ s}^{-1}$



# Chapter 1

## Introduction to the thesis topic

The research field of perovskites has exploded during the last few years. A handful of promising photophysical properties, along with cheap production costs, make these direct bandgap semiconductor materials one of the most interesting materials for future commercial market[8].

Optical properties of perovskites intriguing for solar cell research includes long charge carrier diffusion length along with a broad absorption band. Since the first perovskite solar cell devices were produced in 2009, the power conversion efficiency (ratio between of generated electricity to incoming light energy), PCE, has rapidly improved to reach 22.1 % in 2016[11]. Along with the optical properties, perovskite are easy to manufacture so that solar cell devices results in having low production costs.

However there are currently drawbacks for the potential use of perovskites in technology. Obstacles including instability and toxicity makes the academic community question the extent of the materials future use in solar cell devices. In order to better understand the photophysics of perovskites, more research is needed. My master thesis aims at driving the understanding of the photophysical and photochemical processes in perovskites to a new level.

I have correlated PL microscopy and scanning electron microscopy (SEM) to connect the structural dependence with photoluminescence of methylammonium lead triiodide ( $\text{MAPbI}_3$ ) perovskites. Two different synthesis methods, yielding very different structural properties, are used to prepare samples for investigation.

In this document, Chapter 2 gives some background information and theory about semiconductor properties in general and perovskites in particular. In Chapter 3, the experimental setup is presented together with some specifics about the synthesis methods. Chapter 4 presents some differences in the sample outcome of the two methods.

The main focus of this project has been studying photoinduced degradation of  $\text{MAPbI}_3$  and photoluminescent (PL) lifetimes of different structures. The results from degradation presented in Chapter 5 include photoinduced structural breakdown of the material and the atmospheric dependence on degradation. In Chapter 6, a study of the correlation in structure and PL lifetime is made. Discussion and conclusions about the work performed are presented in Chapter 7 and 8 respectively.



## Chapter 2

# Background information and theory

### 2.1 Semiconductor Fundamentals

The energy structure of a completely pure semiconductor consists of a valence band (VB) and a conduction band (CB) with a forbidden energy level gap of a few eV called the bandgap,  $E_g$ . In its initial state the fermilevel,  $E_F$ , lies within the band gap, indicating that all energy states in the VB are filled with electrons and all states in the CB are empty. Excitation of electrons over the bandgap, e.g. by a photon with high enough energy ( $h\nu \geq E_g$ ), will result in an electron and a hole filling states in CB and VB respectively. The recombination of charges leads to an excess energy, which is either released radiatively (photon) or non-radiatively (phonon or Auger-electron).

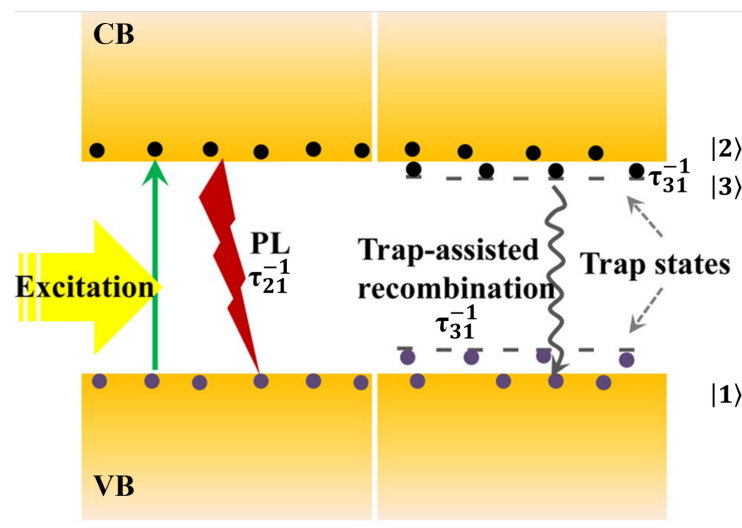


FIGURE 2.1: Energy structure of general semiconductor including trap states. [Picture source: [15]]

There are however often defects in the crystal lattice that will disturb the energy structure of the completely pure semiconductor. Such defects arise from impurities, vacancies or structural irregularities and cause energy structure implication allowing energy states also within the semiconductor bandgap [3]. Figure 2.1 shows the energy structure of a typical semiconductor system, including the band edges and trap levels.

Defect energy-levels that lie close to the band edges (ionization energy of the order of  $kT$ ) are generally referred to as dopants or shallow traps. Defects causing energy levels more towards the middle of the band gap are

considered deep traps. By non-radiative relaxation of minority charge carriers from the CB and VB, the trap states can capture electron and holes, releasing excess energy thermally as lattice vibrations. As a charge has been captured, it can either release its energy non-radiatively or it remains trapped until it is released again (de-trapped).

As mentioned, there are different processes responsible for charge carrier recombination in semiconductors. For example, band-to-band recombination means annihilation of a free electron in the CB and a free hole in the VB, whereas recombination in a localized state is the result of recombination by trap assistance. Energies involved in charges from the bands being trapped are, amongst others, the long range coulomb potential and the energy related to the lattice relaxation in the vicinity of the trap origin. Depending on whether a charge has been trapped or not, rearrangement of the crystal lattice may occur[2].

Another important semiconductor feature is the property of a direct or indirect band gap. In the case of a direct bandgap, the crystal momentum of the valance band maximum (VBM) and the conduction band minimum (CBM) are the same (have the same  $k$ -value in the Brillouin zone). As energy transforms in different forms both the amount of energy and momentum must remain constant. For a direct bandgap semiconductor, excitation/recombination between the CBM and VBM can be done without any change in momentum by just a photon of energy  $h\nu = E_{CBM} - E_{VBM} = E_g$ . In contrast to silicon, perovskites have direct bandgaps, which makes them suitable also as light emitters.

Again, consider Figure 2.1. Each energy state has an average life time before recombination happens. The probability for a specific recombination to happen is simply calculated as the inverse of that lifetime. For an excited electron in the CB there are two transitions possible. Either it could recombine radiative by a band-to-band transition to the VB with a rate of  $\frac{1}{\tau_{21}}$  or non-radiatively to the trap energy state with a probability  $\frac{1}{\tau_{23}}$ . The trap state itself has a lifetime of  $\tau_{31}$  before either non-radiative recombination to the ground state or de-trapping occurs.

Now imagine the case where  $\tau_{21} \ll \tau_{23}$ . This automatically means that excited electrons much rather decay by photon than phonon emission. A material with this property along with a low concentration of traps relative to the concentration of excitation, has high quantum yield. However there is still a chance (very small though) for an excited electron to be trapped in level  $|3\rangle$ , where it stays for an average lifetime of  $\tau_{31}$ . The trap assisted recombination will happen seldom but when it does it is the length of  $\tau_{31}$  that determines when the system again can start to emit light.

## 2.2 Perovskites Properties

Perovskites is a collective name for all compounds with the generic form  $ABX_3$  and a specific crystal structure presented in Figure 2.2. The centre of the unit crystal is occupied by a large atomic or molecular cation (positively charged) of type A. All corners of the unit cell consists of atoms of type B (also cations), while the faces of the cube are occupied by a smaller negatively charged (anion) atom X. In this thesis, synthesis and testing of



the perovskite  $\text{MAPbI}_3$  is made. This is the compound that so far has been used in the most efficient perovskite solar cell devices [12].

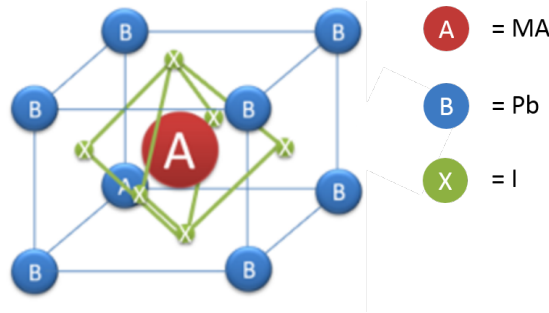


FIGURE 2.2: The crystal structure of a perovskite in the generic form  $\text{ABX}_3$ . Throughout this work  $A = \text{MA}^+$ ,  $B = \text{Pb}^{2+}$  and  $X = \text{I}^-$ . Picture source: [12]

It is due to perovskites broad absorption band and long charge carrier diffusion length that evokes the interest of the materials future use in solar cell technology. Although these promising features have been reported, still irregularities in PL-behaviour (intensity, life-time, luminescent stability) of perovskites targets them as interesting for further investigation to understand more of their photophysical behavior.

Charge carriers generated in perovskite have been reported to recombine through a combination of trap-assisted and direct band-to-band recombination depending on the concentration of traps and excitations. Luminescent lifetime measurements have also given a variation of result in decay features being mono-, bi- or even tri-exponential [4](equation 2.1).

$$\frac{i_{\lambda}(t)}{i_{\lambda}(0)} = \begin{cases} e^{-t/\tau} \\ \sum_{i=1}^n A_i e^{-t/\tau_i} \end{cases} \quad (2.1)$$

In equation 2.1  $\frac{i_{\lambda}(t)}{i_{\lambda}(0)}$  is the relative intensity at time  $t$  of the luminescent sample when excited at wavelength  $\lambda$ . The rows represent mono- and multi-exponential decays where  $A_i$  is the relative contribution of the luminescence from a state with life time  $\tau_i$ .

Large fluctuations of PL intensity, called PL blinking, is a phenomenon typically observed in single dye molecules and other single quantum systems. Digital “on/off” PL blinking has been reported in perovskites quantum dots of about 10 nm in diameter which are close to single quantum systems in their behaviour. Such PL intermittency has been assigned to photo-assisted switching between a charged (‘off’) and a neutral (‘on’) state of the quantum dots. In the charged state, the additional electron in the conduction band absorbs the energy from the recombination events and releases it non-radiatively resulting in suppressed emission – so called non-radiative Auger recombination[6].



## Chapter 3

# Experimental setup

### 3.1 Synthesis

One of the big advantages with perovskites is that a solution based process makes thin film samples easy to synthesize. By variation of the unit structure compounds A, B and X in Figure 2.2 perovskites can have a large range of interesting properties. In the research field of perovskite solar cell devices the goal for physicists, chemists and material scientists has been to develop a synthesis technique that enables fabrication of large area devices with the wanted structural properties.

Two different methods were used for synthesising methylammonium lead iodide ( $\text{CH}_3\text{NH}_3\text{PbI}_3$  or  $\text{MAPbI}_3$ ) throughout this project work. The first involves blending solutions of methylammonium iodide (MAI) and the lead(II) iodide ( $\text{PbI}_2$ ) together. In the other method,  $\text{MAPbI}_3$  is created through a growth process involving lead (II) acetate ( $\text{PbAc}_2$ ) in a solution of isopropanol (IPA) and MAI.

Below follows a brief description of the the synthesis methods. The full recipe description follows in Appendix A.

#### 3.1.1 Method 1

The first step is to dilute  $\text{PbI}_2$  and MAI separately in dimethylformamide (DMF). 460 mg of  $\text{PbI}_2$  (molar weight 587.9134g/mol) and 160 mg of MAI (158.97 g/mol) were each blended into a volume of 1.25 mL DMF creating a concentration of 0.8 M. After the separate solutions had diluted properly they were blended together [1:1] and put to stir with a magnet at a hot plate (60°C) for 8h.

After completing the development of  $\text{MAPbI}_3$  the liquids could be investigated in the PL-setup after a sample preparation resulting in solid  $\text{MAPbI}_3$  on glass plates. By using DMF for diluting, it was possible to choose the concentration of the thin film. Throughout the experiments performed in this project, the samples prepared are either 100 % so called "bulk samples" or low concentration samples of  $\leq 5$  %.

In the sample preparation, 200  $\mu\text{l}$  of  $\text{MAPbI}_3$  (non-diluted or diluted) liquid was placed on a clean glass plate and spin-coated at 1500 rpm for approximately 1 minute before they were annealed on a hot plate at 80°C for 30 minutes. The annealing was done in a foil box in order to not expose the samples to light.

### 3.1.2 Method 2

In the second method (M2) of synthesis, 100 mg of  $\text{PbAc}_2$  was dissolved in 1 ml of miliQ water. The solution was then dropped on a glass slide and left to bake for 30 min at  $65^\circ\text{C}$ . After baking, the glass plate was put in a petri dish with a liquid solution of dissolved MAI in isopropanol (IPA) (40 mg in 1 ml). The reaction was left to happen in room temperature for 20 h, not exposed to light. After drying the product in  $\text{N}_2$ , it was possible to use a soft tissue to scrape  $\text{MAPbI}_3$  crystals from the outer layer of the samples. The crystals were placed on a clean glass plate in order to investigate them with the fluorescence microscope.

## 3.2 Instrumental Description

### 3.2.1 PL-measurement Setup

Figure 3.1 shows a sketch of the microscope used during PL-measurements. The choice of whether the Argon (CW) or the diode laser (pulsed) should be used depends on the aim of the experiment. The pulsed diode lasers (at different wavelengths) are used for lifetime-measurements.

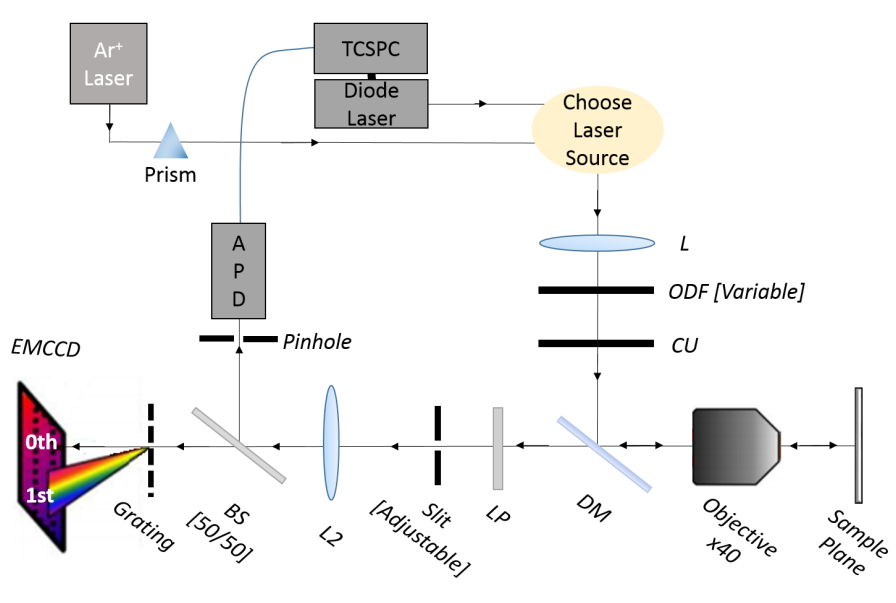


FIGURE 3.1: A sketch of the setup used in the PL-measurements.

The argon-laser consists of multiple wavelengths that are spatially separated by a prism. In the following experiments, the lines at 514 nm (green color) and 458 nm (blue color) were used (the green laser having higher excitation power).

The laser beam in use passes a lens ( $L1$ ), an optical density filter ( $ODF$ ) a laser clean up filter ( $CU$ ) and a dichroic mirror ( $DM$ ) before reaching the sample. The function of the lens ( $L1$ ) is to decollimate the beam so that the focus of the laser does not align with the sample plane. The advantage of the slightly defocused laser in the sample plane is that it enables wide-field imaging. The laser beam cross section illuminating the sample plane has an

approximate diameter of 30  $\mu\text{m}$ . The adjustable optical density filter (*ODF*) makes it possible to adjust the excitation power density in the experiments.

The clean up filter and dichroic mirror in the setup are design to only let light in a very narrow band around the laser wavelength excite the sample. The filter (*CU*) simply blocks unwanted excitation light, while the dichroic mirror in use are designed only to reflect light at a very accurate band centered at the laser wavelengths. Other wavelengths pass the mirror without change. There is a possibility to change the atmosphere of the sample being studied using a nitrogen gas chamber.

As the laser light has excited the sample fluorescent light passes the inverted dry objective lens (40 $\times$ Olympys LUCPlanFl, NA = 0.6). The fluorescent light then passes the dichroic again (*DM*), which again reflects light around the laser wavelength. Lights of other wavelengths passes the *DM* without change. The long pass filter (*LP*) placed after the dichroic cleans up the fluorescent light further, ending up with light only with  $\lambda > \lambda_{LP}$  getting magnified  $\times 2$  by a lens (*L2*) and then detected. This in order to block out the laser light and surface reflection from being detected.

Detection of the fluorescent light is made either by an RGB camera (Nikon) giving colored images or with an Electron Multiplying CCD camera (Princeton Instruments, ProEM). A beam splitter (*BS* [50/50]) can also be switched on to direct part of the beam to an Avalanche Photo Diode (*APD*). In experiments with the CW Ar<sup>+</sup>-laser, only the CCD is used and in lifetime-measurements the APD will be needed.

### CCD-measurements

The CCD gives a black and white image of 512 $\times$ 512 pixels. The magnification factor in the CCD detection plane is 80, from the combined lens  $\times 2$  and the objective lens  $\times 40$ . Each pixel has a physical side measure of 1.6  $\mu\text{m}$  which corresponds to an effective side of 200 nm in the image. The signal from the CCD is monitored and analysed in WinSpec Princeton Instruments Spectroscopy Software. Using WinSpec settings gives the possibility to either take single images of the detected light or to record a movie by a series of 1000 images with a chosen exposure time of 100 ms each.

By using the adjustable slit in the setup the beam can be narrowed along the horizontal direction. By switching on a transmission grating (150 lines/nm) in front of the CCD, the spectrum information from the zeroth and first-order diffraction can be seen in the pixel window. Therefore, the spectral information from a particular luminescent object in the image can be acquired. From measurements from a fluorescent tube with known spectrum the CCD was calibrated to correspond to a horizontal value of 2.16 nm/pixel.

### Method of Reaching Super Resolution

In order to reach beyond the light diffraction limit of the microscope, Mat-Lab was used to develop a program that could reach a resolution of  $< 10$  nm from luminescent samples. The user simply chooses one pixel on the CCD around which an area of 7 $\times$ 7 (adjustable depending on size of luminescent object) is cropped and analyzed to fit a 2D Gaussian function, equation 3.1 and 3.2.

$$G(x, y, \theta) = A \exp(-(a(x - x_0)^2 + 2b(x - x_0)(y - y_0) + c(y - y_0)^2)) \quad (3.1)$$

$$a = \frac{\cos^2 \theta}{2\sigma_x^2} + \frac{\sin^2 \theta}{2\sigma_y^2}, b = \frac{\sin 2\theta}{4\sigma_x^2} + \frac{\sin 2\theta}{4\sigma_y^2}, c = \frac{\sin^2 \theta}{2\sigma_x^2} + \frac{\cos^2 \theta}{2\sigma_y^2} \quad (3.2)$$

The Gaussian fitting gives more accurate localization of the emitting object by the values of  $x_0$  and  $y_0$ , indicating the maximum intensity of emission profile in the image plane. The emission profile shape is determined by the standard deviations  $\sigma_x$  and  $\sigma_y$  along with  $\theta$  indicating the angle between the  $x$  and  $y$ -axis of the Gaussian beam profile. With the relative standard deviation  $\sigma_x/\sigma_y$  one could make conclusions about the shape of the luminescent source of the emission. A symmetric emitting object ( $\sigma_x/\sigma_y \approx 1$ ) originates from a point source, whereas a Gaussian bead with a relative standard deviation that differs much, generally originate from a more oblong shaped source.

Using the CCD to record a movie of the luminescence when studying the blinking features of perovskites it is possible to follow how the Gaussian profile of the emitting object changes in time.

### Time-Correlated Single Photon Counting (TCSPC)

Lifetime measurements are done using Time-Correlated Single Photon Counting (TCSPC) using PDL 828 "Sepia II". This technique uses a pulsed laser and a single photon detector to build a histogram corresponding to photon counts vs. the time between the triggering of the excitation pulse and the time of detection, see Figure 3.2. Due to the fact that a single photon yields a very small intensity, the Avalanche Photodiode (APD) is needed in order to connect the intensity to a voltage high enough for analog detection. The data can later be fitted to an exponential decay curve to calculate the average luminescent lifetime of the object studied.

Determination of the time-resolution,  $\Delta t_{TCSPC}$ , of the TCSPC detection is dependent of frequency  $f$  of the excitation pulse used and the number of "time bins" for the stop-watch in the single-photon counter, see equation 3.3. The photon counter used in our setup has  $n = 12500$  channels and as it is switched between a frequency of  $f_1 = 5$  MHz and  $f_2 = 2.5$  MHz during the experiments the time resolutions differ between 16 and 32 ps for the respective frequencies.

$$\Delta t_{TCSPC} = \frac{1}{nf} \quad (3.3)$$

The time resolution of the entire system (which dictates the information we can get) depends on the instrument response function, which is a measurement of how long it takes for the photon to travel from the sample to the detector and also how long it takes the excitation photon to reach the sample.

Using the Sepia II software it is also possible to measure a "movie" of the lifetime by recording the average lifetime of photons being detected within a frame of various time intervals.

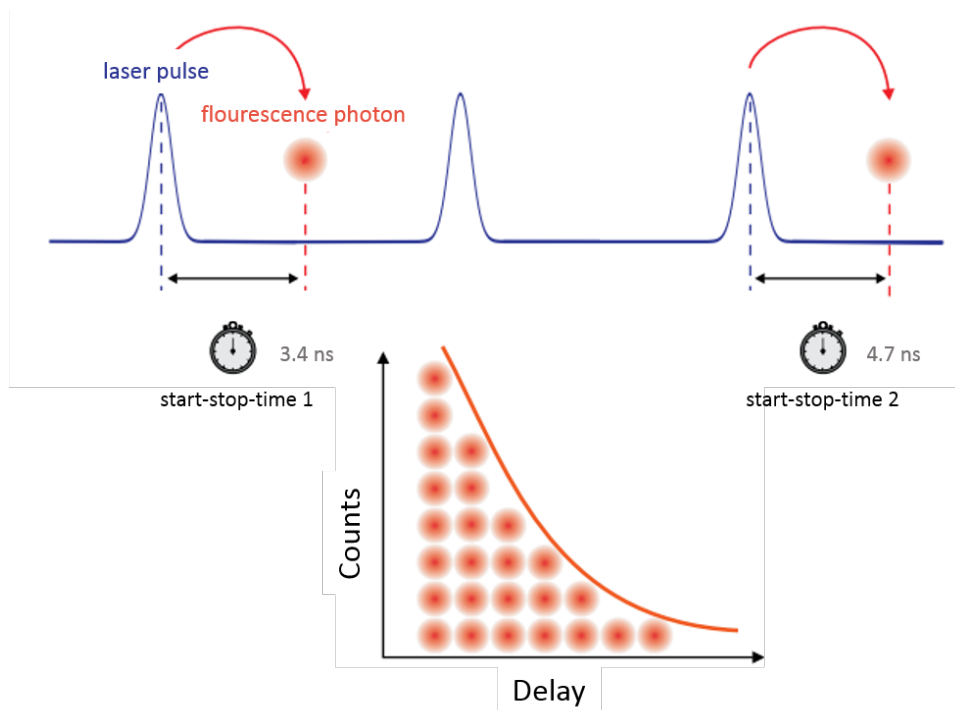


FIGURE 3.2: The principle of TCSPC fluorescent lifetime measurements. A single photon counter is used to build a histogram of photon counts per time-channel. Picture source: [18]

A pinhole ( $50 \mu\text{m}$  physical size, effective size  $0.63 \mu\text{m}$ ) is placed in front of the APD. The reason is that detection of the luminescent life-time should correspond to the light from only one emitting object on the sample. By alignment of the laser passing the pinhole and the CCD one can choose for which object the lifetime should be detected.

### 3.2.2 Scanning Electron Microscope

Connecting the structure and the photoluminescence of  $\text{MAPbI}_3$  perovskites, the Scanning Electron Microscope (Hitachi SU8010 Cold Field Emission SEM) at NanoLund (Fysicum, Lund) was used. After the collection of PL-data was finished, the samples were sputtered with Platinum Pt to get conductive surfaces. High resolution images of  $1.0 \text{ nm}$  @  $15\text{kV}$  of the surface topography were obtained.

By overlapping information gained from the RGB and CCD cameras with the topological SEM images it is possible to connect structural differences with photoluminescent differences of  $\text{MAPbI}_3$  perovskites. Throughout this project work, structural data has been connected to different synthesizing methods (Chapter 4) bulk degradation (Chapter 5) and the large variation of luminescent life-times of different  $\text{MAPbI}_3$  structures (Chapter 6).





## Chapter 4

# Results of Different Synthesis

Samples from both preparation methods were used in the experimental work of the master thesis projects. The difference in optical and structural properties between samples from the different methods was shown to differ substantially, which motivated a chapter dedicated to the differences in the outcome of the synthesis processes.

Figure 4.1 shows the SEM images of the typical topology of three different samples. (a) and (b) are from M1 with a 100 % and a 3 % dilution concentration respectively. Figure (c) shows the typical, more crystalline result of M2. Zoomed in images of two clusters from the low-concentration M1 sample and from one crystal from the M2 sample are shown in (d-e) and (f) respectively.

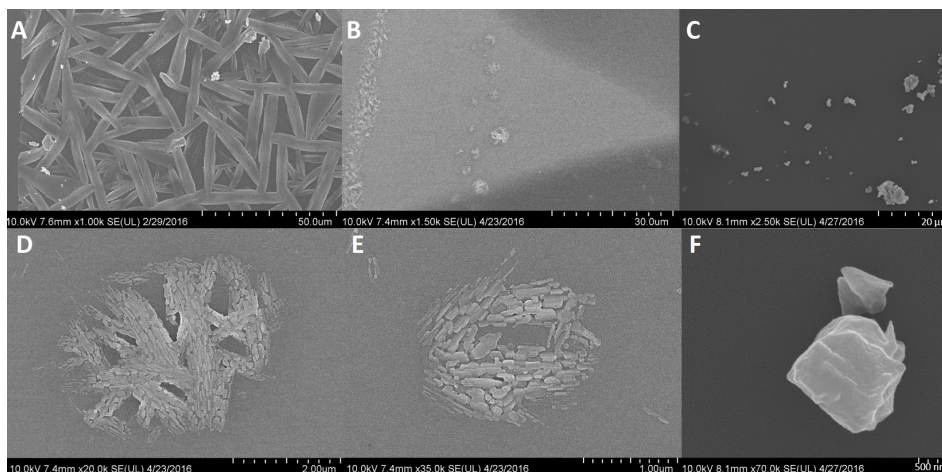


FIGURE 4.1: A comparison of structural results of synthesizing method 1 and 2. (a) 100 % prepared with M1 (b) 3 % prepared with M1. (c) M2. (d)-(e) Zoom in of two clusters from 2 % M1 sample. (f) Zoom in of crystal from M2 sample.

Structural inhomogeneity is evident in all samples, regardless of preparation method. However the 100 % M1 bulk sample shows to have a very irregular and badly covered thin-film structure. The diluted, low-concentration sample, also result in the "straw-like" structural shape of the perovskites with the difference of being spread out in clusters of different sizes. One explanation to the inhomogeneous resulting shape of the bulk and clusters from M1, is that the annealing process of  $\text{MAPbI}_3$  in M1 happens first after the glass plate (on which the liquid including the reactants are spincoated) is placed on the hotplate. Thus the annealing process will depend largely on properties like temperature, annealing time, atmosphere etc..

Crystals of more uniform shape is maintained from the second method M2. In this method the annealing process happens during the 20 h that the glass plate (containing a solid mix including Pb) is left in the vial (containing a liquid solution of MAI). Thus the annealing conditions for each crystal structure has higher resemblance than in M1. Although the crystals visualized in Figure 4.1(c) are not completely homogeneous, the surface of each and every crystal is more even. Also the crystals obtained from M2 are smaller compared from the zoomed in pictures in 4.1 (d-f).

A main goal of this project work was to investigate the structural influence of the optical properties of MAPbI<sub>3</sub>. In the degradation and life-time experiments described in Chapter 5 and 6 respectively, it is therefore clearly described which preparation method that was used for the sample under investigation. Also, within the sample the PL properties varied from cluster to cluster and crystal to crystal. With this chapter in mind the reader has been provided with an overview of the typical sample structure.

## Chapter 5

# Degradation of Bulk Samples

### 5.1 Photoinduced Degradation Process

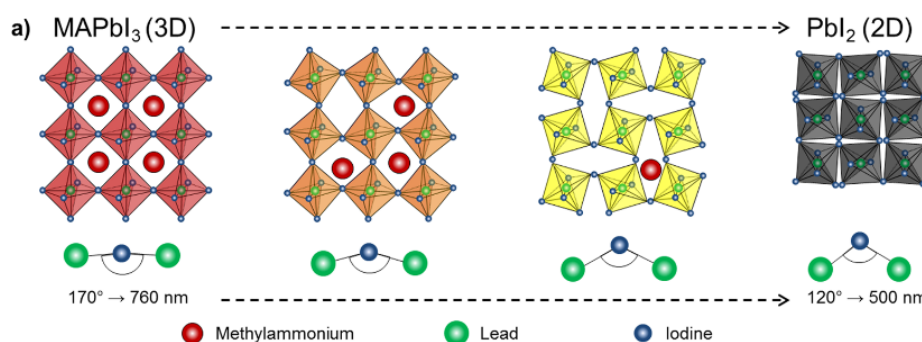


FIGURE 5.1: Structural deformation of the 3D crystal of  $\text{MAPbI}_3$  to the 2D crystal of  $\text{PbI}_2$ . Picture source: [1].

The process of photoinduced degradation of methylammonium lead triiodide in air has recently been described by the migration of  $\text{MA}^+$  ions through the crystal causing the perovskite crystal structure to deform. What causes the ions to migrate seems to be through overcoming the kinetic activation barrier allowing ions to diffuse by vacancies of  $\text{MA}^+$  in the structure. As  $\text{MA}^+$  leaves the 3D crystal structure the Pb-I-Pb bonding angle tends to decrease. The successive process ending up with a 2D crystal structure of  $\text{PbI}_2$  is visualized in Figure 5.1. The transformation gives rise to a spectral blue-shift, a shift of emissive localization point and an luminescent intensity drop. The largest shifts happen as the PL-intensity has dropped to about 30 % of its initial value [1],[19].

### 5.2 Experimental Description

A bulk sample (M1) was prepared to investigate the photoinduced degradation process of  $\text{MAPbI}_3$  in air. As degradation laser, the CW higher power 514 nm line of the  $\text{Ar}^+$  was used. After degradation was completed an investigation of fluorescence from both  $\text{MAPbI}_3$  and  $\text{PbI}_2$  could be performed using a blue laser of shorter wavelength 458 nm and lower power. The blue laser is needed since the green laser photon energy provides no excitations over the 2.4 eV (516 nm)[16]  $\text{PbI}_2$  bandgap. The fluorescent peaks of  $\text{PbI}_2$  and  $\text{MAPbI}_3$ , lies at approximately 500 nm (green) and 770 nm (red) at room temperature [1]. The fluorescent spectrum of  $\text{MAPbI}_3$  and  $\text{PbI}_2$  can be seen in Figure 5.2, where also the experimental setup lasers are marked.

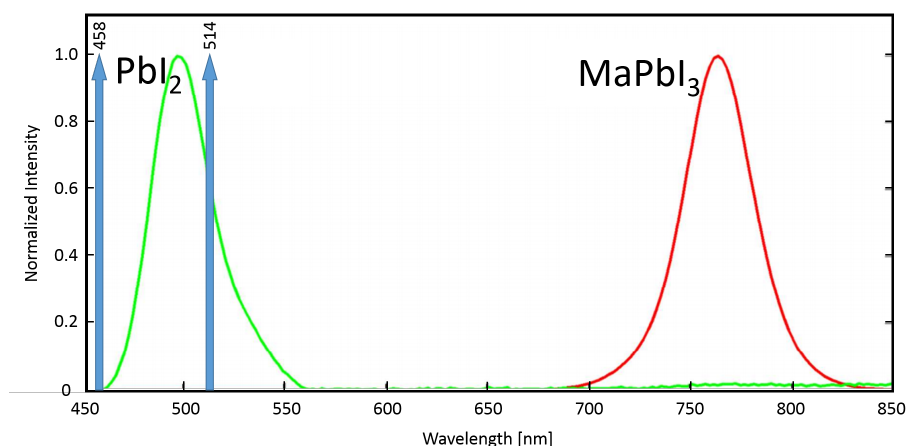


FIGURE 5.2: PL spectrum showing features of importance during degradation experiments. The fluorescent peaks of MAIPbI<sub>3</sub> and PbI<sub>2</sub> are visualised together with the laser wavelengths at 458 and 514 nm. Picture source: [1]

Figure 5.3 represent a concluding scheme of the outcome of a degrading process in air.

### 5.2.1 Spectral difference

The fluorescent differences before and after degradation in air are presented in Figure 5.3 (a) and (b). The cross section at which the green laser has been illuminating the sample, has transformed the fluorescence from red to green. This is explained as photons from the laser induces excitations over the MAPbI<sub>3</sub> bandgap creating free charge carriers of electrons and holes in the respective bands. The charge generation results in a non-equilibrium state with an electric-field gradient causing MA<sup>+</sup> ions to migrate through the bulk resulting in the transformation to PbI<sub>2</sub> [1].

Figure 5.3 (e) visualizes that the degradation has also caused a change in absorption for the bulk sample. This RGB picture was taken by just illuminating the sample with a normal light bulb, detecting the absorption.

### 5.2.2 Structural Difference

In an SEM investigation of the area, resulting in the image in Figure 5.3 (c), it was possible to draw conclusions also about a structural change of non-degraded vs. degraded areas of the bulk. The former reveals a somewhat less "cracked" surface structure than the latter, Figure 5.3 (d). This result is a further evidence of the migration of ions during the photoinduced degradation process in air, causing the crystal structures to deform and migration pathways to be generated by open space and wrong bonds at grain boundaries in the bulk. Even though the Pb-I-Pb bond-angle changes on a nanometer scale, the result of the break down can be seen in larger areas that are affected.

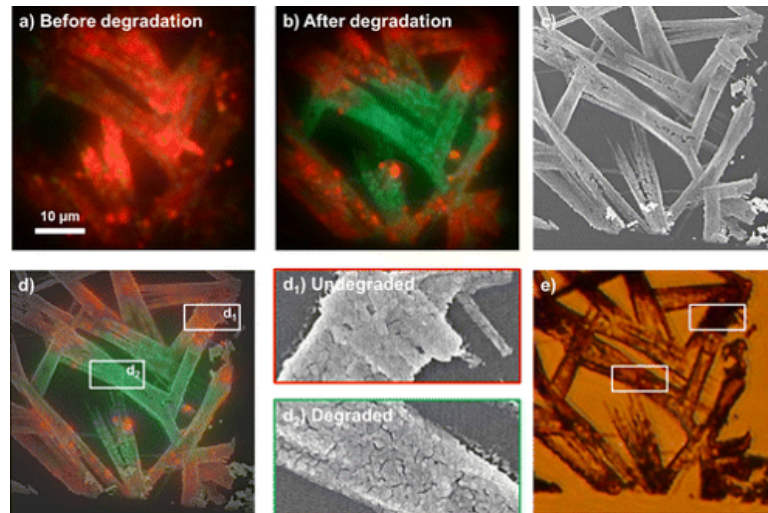


FIGURE 5.3: Summation of resulting differences before and after degradation of MAPBI<sub>3</sub> in air. The spectral change before and after degradation is clearly observed by the fluorescence captured by the RGB camera in (a) and (b). An image of the structure of the area is shown in (c). Overlapping the RGB and the SEM of it made it possible to distinguish a slight difference in crystalline structure between degraded and undegraded crystal structure. The difference in absorption for the degraded area is also shown captured by the RGB with the background light of a halogen lamp in (e).

### 5.3 Atmospheric dependence: Air and N<sub>2</sub>

Photoinduced degradation of MAPbI<sub>3</sub> happens through different processes in air and nitrogen. This was concluded after degrading an area with the 514 nm CW laser in, firstly, a nitrogen atmosphere and thereafter in air, recording the entire experiment procedure in one RGB movie. Snapshots from the movie at  $t = t_i$  ( $i = 1-8$ ) are cropped out and visualized in Figure 5.4. The lasers used for excitation are labeled above the columns and the rows represent different atmospheres.

Since no green fluorescence and no change in absorption is evident after degrading the sample in a nitrogen atmosphere it was concluded that the degradation of MAPbI<sub>3</sub> in N<sub>2</sub> happens through a different mechanism than ion-migration of MA<sup>+</sup> and crystal deformation in air. We conclude degradation still occurs in N<sub>2</sub> since an intensity drop is observed.

### 5.4 Degradation at Higher Power

Degradation also at a higher power in excess of 1000 W/cm<sup>2</sup> was performed. This process turned out, not only to happen faster than the former degradation process but also to have different results.

By excluding the decollimating lens in the experimental setup 3.1 the green laser was focused in the sample plane providing a laser spot with a 100 times higher power density than the former. As the focused laser was moved to burn a line in the bulk sample, an RGB movie was recorded. In

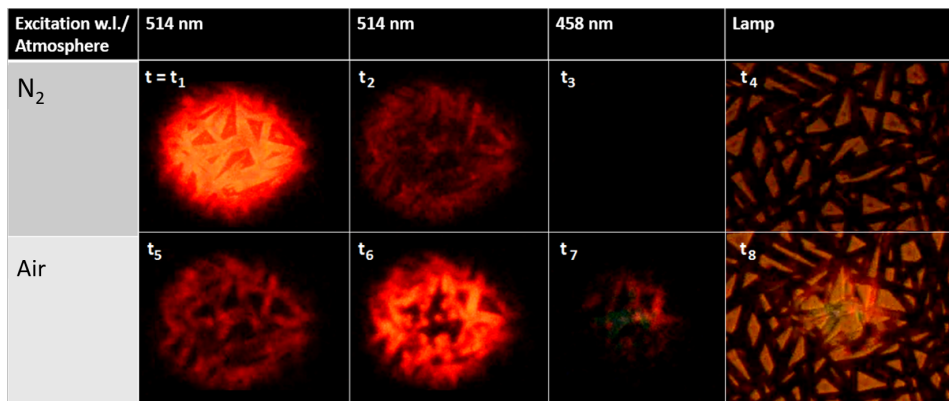


FIGURE 5.4: Picture showing the difference in degradation in nitrogen vs. air. The same area was degraded in different atmospheric conditions. In nitrogen in the upper row and in air in the bottom. From left to right you see the area illuminated with the 514 nm laser first before degradation and then also after degradation. In the third column the 458 nm laser is used for illumination after degradation and in the fourth column the absorption of the area is shown when illuminated with a normal light bulb.

the RGB movie it became clear how the bulk degraded within a time frame of one second. Using the blue laser for illumination it was concluded that in this degradation process no transformation of  $\text{MAPbI}_3$  to  $\text{PbI}_2$  could be observed since the degraded line was left completely non-luminescent.

#### 5.4.1 Structural difference

PL-results combined with SEM images made it possible to make connections between luminescence and structural difference. In the overview SEM image (Figure 5.5) a clear structural difference between the burned line and the bulk can be seen. The high-power laser has split the bulk structure into small separated clusters with sizes of around a few microns.

Evident from this experiment is that the higher power laser does not speed up the mechanism of a successive transformation of  $\text{MAPbI}_3$  to  $\text{PbI}_2$ . Instead, a too high excitation power kills the sample. A discussion of which material the degraded line consist of follows in Chapter 7.

#### 5.4.2 Surviving Intensity Oscillating Area

An interesting discovery was detected in the high power degradation process. One specific area inside the otherwise dark line maintained its luminescence also after the degradation, Figure 5.6 (a). The image is a snapshot from a movie recorded by the CCD camera showing that the area contained small luminescent structures.

A further investigation of the area showed that the small spot structures in the area had been differently affected by the degradation laser, some being completely destroyed as light emitters while others still emitted red fluorescent intensity. Figure 5.6 (b) shows how a more "grainy" structure is associated with a non-luminescent area, while structures of more smooth surface (Crystals 1 and 2) maintain their luminescence.

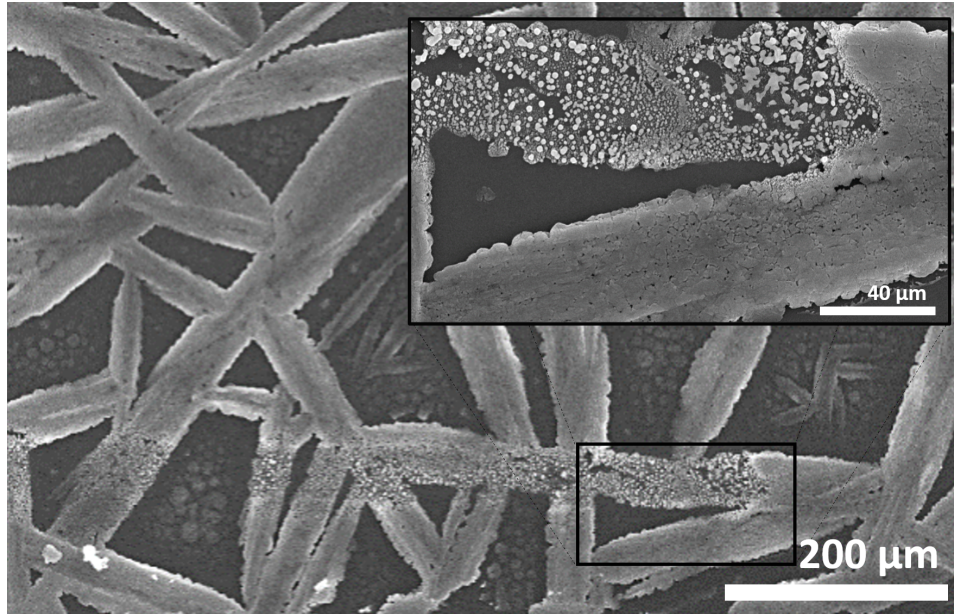


FIGURE 5.5: SEM image of high-power-laser-degraded line. The structural breakdown is evident both in the zoomed out picture and in the inset of zoom in of the the marked area.

Further investigation of the luminescence from the crystals marked 1 and 2 in Figure 5.6 (b), we detect a feature newly discovered by us for perovskites: Oscillating intensity. The oscillating feature of Crystal 1 and 2 along with a cropped out area of the bulk from the same CCD movie are plotted in Figure 5.6 (c). Evident is that the bulk area does not show the same oscillating behavior as the surviving crystals and also that the oscillations from the two crystals are slightly out of phase. This means that the oscillation is *not* a result of an artifact in the measurements (mainly from fluctuations of the laser) but is connected to the difference in PL properties for the bulk and smaller structures.

Apart from the oscillating intensity feature, the crystals also show some blinking behaviour, e.g. Figure 5.6 (c). Using the super-resolution method described in Chapter 3 the intensity variation could be connected to an emitting point with a resolution below 10 nm. Analyzing the blinking of Crystal 2 in Figure 5.6, the switching between on and off intensity stages was connected to a "jump" in the localization point of approximately 100 nm (Figure 5.7). It seems like blinking happens as one part of the crystal completely quenches, i.e. suddenly stops emitting light or in other words recombine radiatively. These results are discussed to be connected to localized traps in Chapter 7.

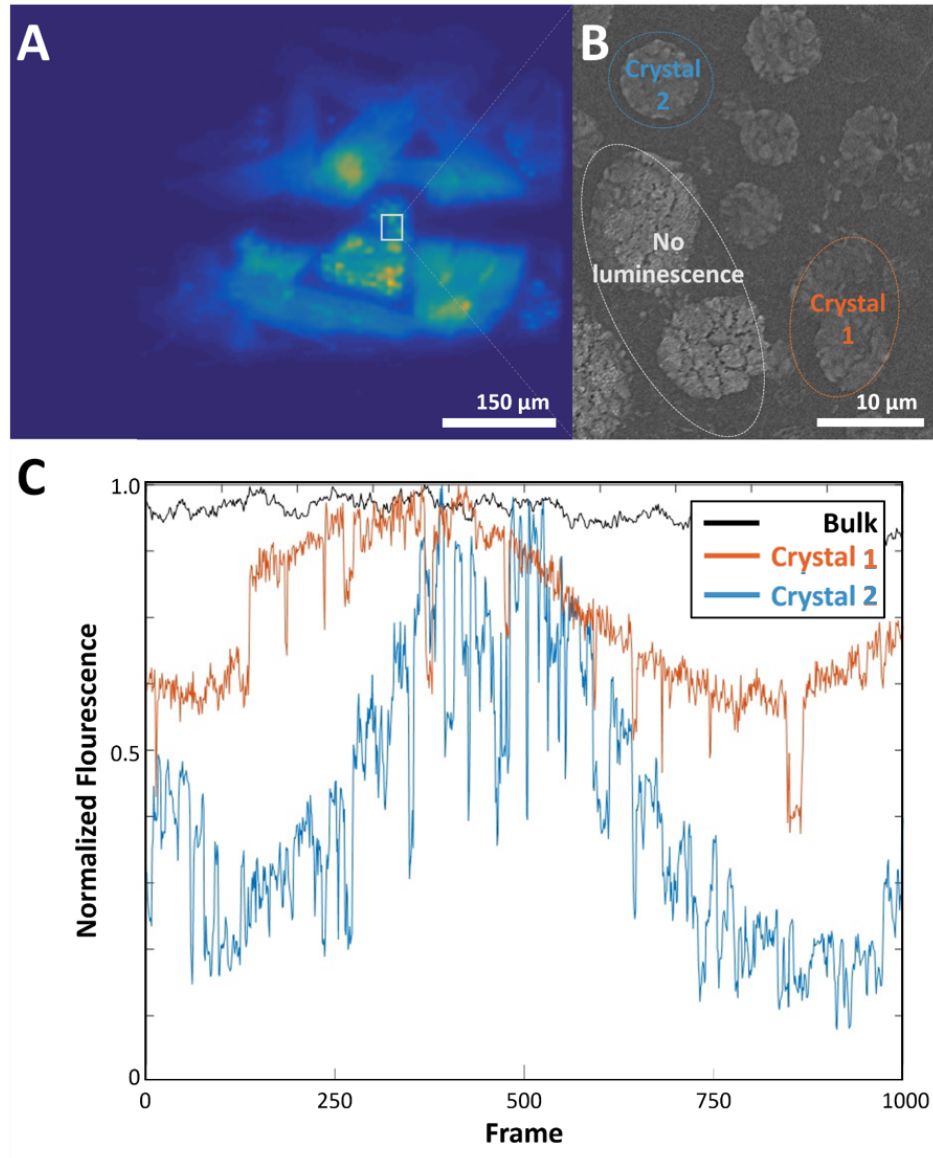


FIGURE 5.6: Concluding information of the surviving area after degradation. a) CCD image of high-power degraded area showing luminescent surviving area [Excitation laser: 514 nm]. b) Zoom in if the small structures indicating non-luminescent and luminescent structures. c) Intensity profile in time for the two luminescent crystals marked in b) along with a cropped out segment of the bulk in the same movie recording.



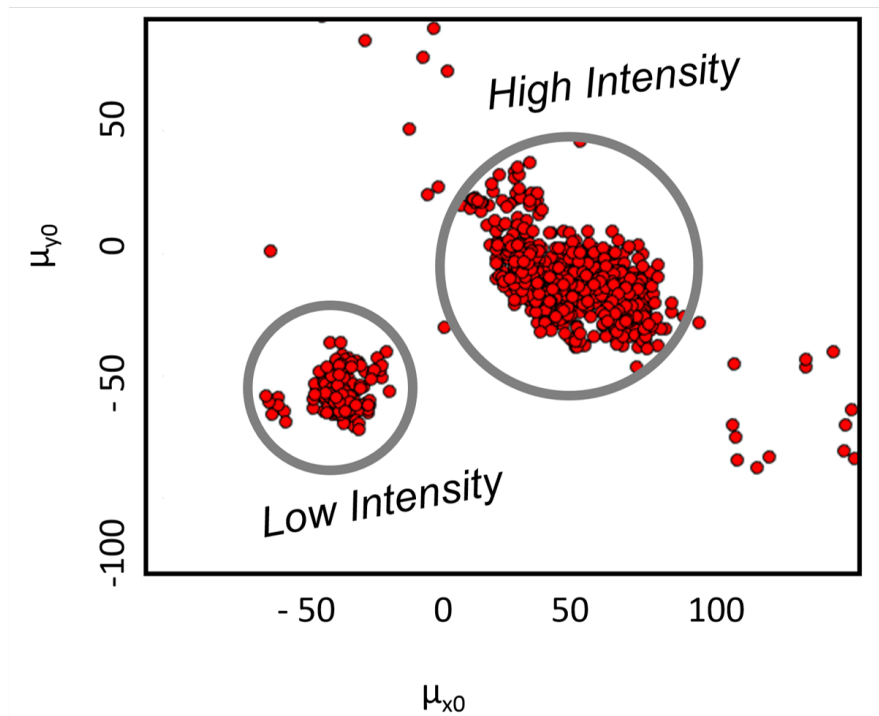
**Variation of position of average emission profile for Crystal 1**

FIGURE 5.7: Using super resolution the blinking has been connected to a position change of the emissive point.



## Chapter 6

# Life-time Measurements of MAIPbI<sub>3</sub>

### 6.1 Background of Luminescent Lifetime

In the last experimental section, investigation of the luminescent decay of different sample structures were investigated. The aim of the experiment was to connect different structural shapes to different luminescent lifetimes. For future aspects, if perovskites are to be used in high-efficient commercial solar cells, the wanted properties are long charge carrier diffusion length to get high current rate from solar light excitation. The diffusion length is directly connected to mobility and the lifetime of the charge carriers in their respective bands.

Traps limit the mobility and thereby the effective PCE of the solar cell. Since we want to understand how traps relate to various structures, PL lifetime measurements becomes an important tool.

Depending on parameters like excitation power and wavelength along with temperature and sample size various results have been reported for the luminescent lifetimes of MAPbI<sub>3</sub> perovskites. Apart from a large variation of PL lifetimes [5, 17], durations the decay profiles have also been reported to be both mono- and multiexponential. Multiexponential decay indicates that more than one energy level is included in the process of recombination [13].

### 6.2 Structural dependence of lifetime

In the lifetime measurements samples from both synthesis methods were used. Emission from different clusters and from M1 and crystalline structures from M2 were one by one aligned to be detected by the APD in TCSPC measurements. The diode laser provided excitation pulses with a duration of around 100 ps/pulse.

Figure 6.1 shows the lifetime data for some selected sample structures. The SEM images shows a cluster from M1 6.1(a) along with two different shaped structures resulting from M2 6.1 (b) and (c) of approximately the same size. In Figure 6.1 the luminescent decays of the different structures are presented.

Differences in luminescent lifetimes is obvious and with the correlated SEM and lifetime results it is possible to connect shorter lifetimes with a more irregular structural shape. The much longer lifetime of 190 ns is connected to the most homogeneous structure in 6.1 (c).

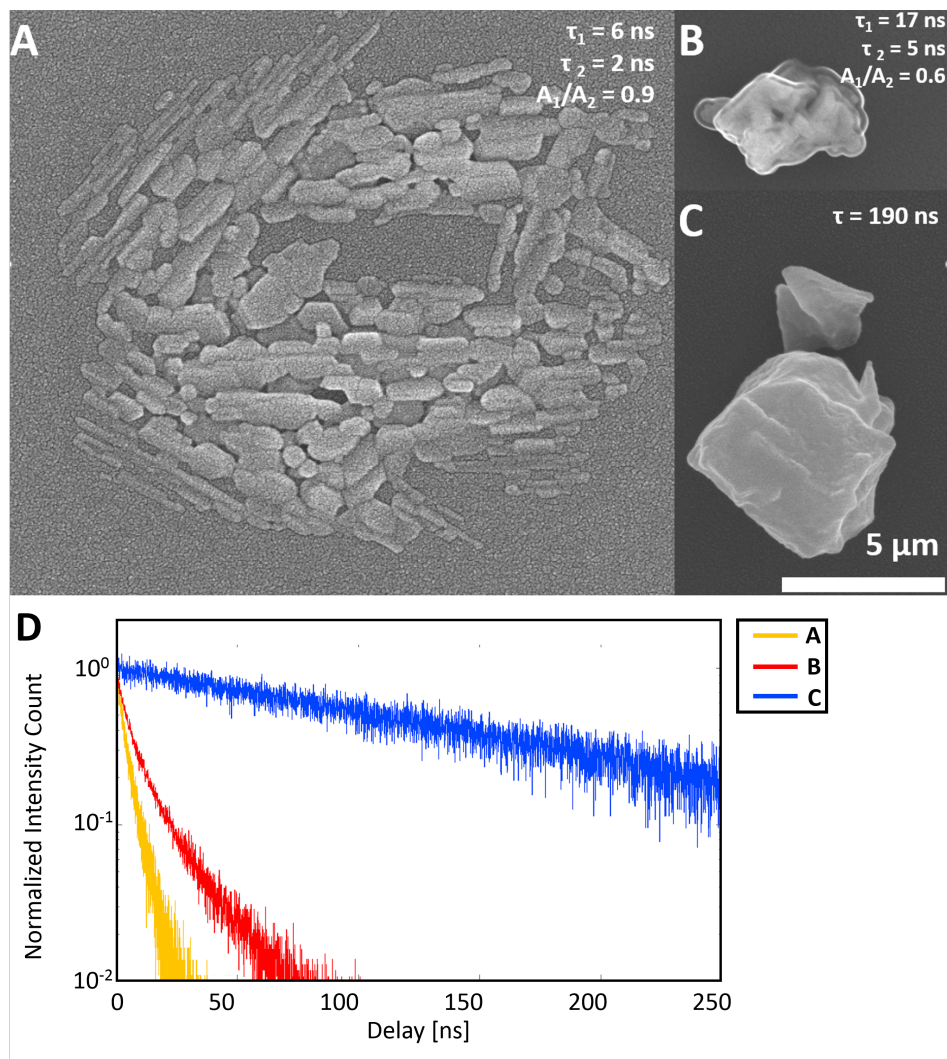


FIGURE 6.1: Image showing results from the lifetime measurements. (A) Crystal from low concentration sample from M1. (B)-(C) Are two crystals from M2. The lifetimes and relative amplitudes are presented each SEM image. (D) Shows the decay curve of the three different structures.

Also, the *decay profiles* are different for the different structures. The long lifetime structure was fitted with a monoexponential decay curve, while the shorter lifetime decays seems to be biexponential. The latter reveals more than one recombination process for excited electrons and holes, equation 2.1.

It is obvious that the crystals from method M2 resulted in structures with very different lifetimes (e.g. Figure 6.1 (b) and (c)) but also the different structures of M1 showed a large variation of measured luminescent lifetimes. Bigger islands with higher height (normal to the sample) and bigger volume appeared to have longer lifetimes reaching above 20 ns, while smaller more "flat" structure had lifetimes below 10 ns. Examples of a longer and a shorter lifetime cluster can be seen in the zoomed pictures in Figure 4.1 (d) and (e) in Chapter 4.

### 6.3 Blinking Structures

Samples from both synthesizing methods proved to have unstable blinking structures at a varying rate. Apart from the bulk the blinking structures maintained a high intensity for a longer time of illumination with the 514 nm laser. In other words they did not degrade while blinking. This is in accordance with [1] which explains how the degradation is put on hold when the crystal blinks "off".

By observing a single blinking structure and recording the luminescent lifetime for a series of frames it was possible to connect the "on" and "off" stages of the intensity to different lifetimes. The result for two different crystals from M2 are presented in Figure 6.2.

Lifetimes for the "on" and "off" stages are calculated as an average for those frames within the intervals marked in the intensity plot to the left in Figure 6.2. It is clear how the switch to a lower intensity level corresponds to a shortening of the luminescent lifetime.

Also the lifetime from the two different blinking structures seems to differ a lot which is a result of the general unreliability of different perovskite crystals.

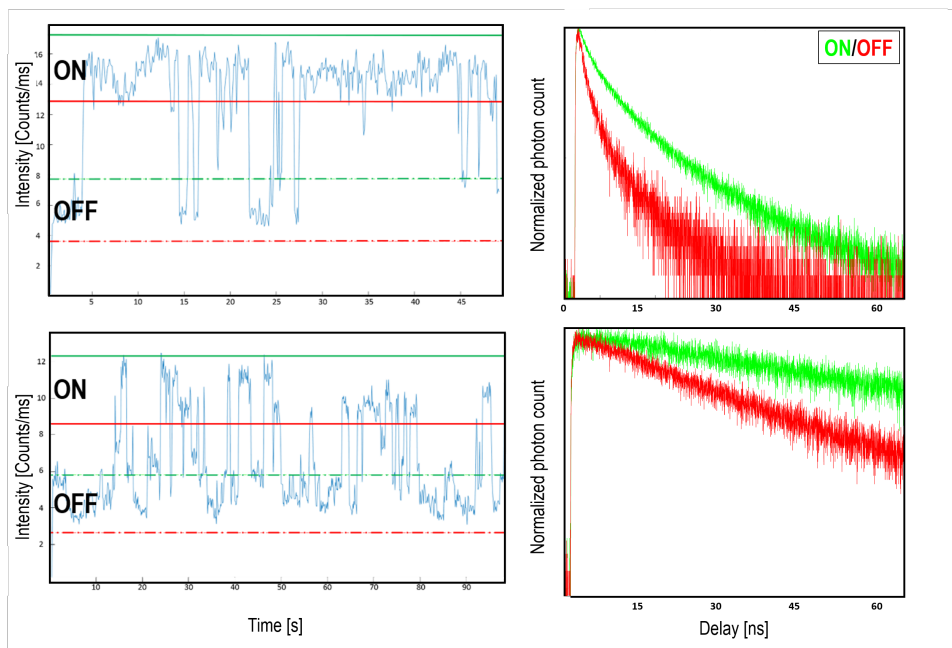


FIGURE 6.2: Separation of lifetime measurements for the on and off stages for two blinking structures.



## Chapter 7

# Discussion of the Experimental Results

### 7.1 Synthesis

Throughout the results it is clear that both methods for synthesizing perovskites yields structures with very different properties. M1 produces bulk samples with very inhomogeneous structure and small blinking areas or clusters of a few microns with a very irregular surface. Benefits of this synthesizing technique include the fact that the inhomogeneity of the samples provides a large distribution of structures and phenomena for perovskite investigation.

The result of M2 shows structures of a few hundred nanometers, which had more even surfaces. Crystals from M2 also showed by observation to be more stable when it came to photoinduced degradation. The variation in optical properties between clusters and crystals in the same sample connected optical properties of  $\text{MAPbI}_3$  to be structure dependant.

### 7.2 Degradation of Bulk Samples

First consider the experiment of degradation. In air it was concluded that the mechanism that transforms  $\text{MAPbI}_3$  to  $\text{PbI}_2$  is the migration of  $\text{MA}^+$  ions, causing the Pb-I-Pb bond angle to decrease. Migration happens as the laser light makes ions overcome the kinetic energy barrier of diffusion to make them diffuse to out of the laser beam area by e.g. vacancy of ions in the surrounding. In order to make ions migrate, the force of the field must be high enough (there must be enough excited charges) to overcome the binding force of the  $\text{MA}^+$  in the unit crystal lattice.

The results from the degradation experiments show that the degradation occurs in the center of the laser, where the laser has the highest intensity. This agrees with the ion-migration theory, since the charge build up is higher in this area.

The results of the RGB pictures in Figure 5.3 shows edges and dots in the otherwise degraded bulk area, still emitting red fluorescent light. No ion migration process has taken place from these sites, since the excitation power was not high enough. Comparing with the SEM images, no clear structural similarity can be seen, but the fact that these sites still consist of  $\text{MAPbI}_3$  may be because the surrounding crystal do not have many  $\text{MA}^+$  ion vacancies.

### 7.2.1 Degradation at Higher Power

Now onto a discussion about which material the line after high power degradation process consist of. For MAPbI<sub>3</sub> perovskites the orbitals of the valence band maximum (VBM) and the conduction band minimum (CBM) in the energy structure are well understood. The VBM is an antibonding combination of covalent character between Pb-6*p* and I-5*p* orbitals. Also CBM is an antibonding combination between Pb *np* and I *ms* orbitals, however this bonding is more ionic with the Pb orbitals contributing to around 80 % of it [14]. As higher power degradation is preformed it is tempting to imagine that the exciting power is high enough to break the ionic bonding between the iodide and the lead atoms. As photoexcitation couples electrons from the iodide to a lead atom, the non-luminescent line left after high power degradation suggestively consists of these two materials separated.

In the high power degradation line, one area of smaller structures partly maintained their luminescence after the laser burning. Further investigation showed a clear structural difference between non-luminescent and luminescent islands. One explanation to why some structures are kept intact could be their smaller height compared to the bulk. If light-matter interaction for the process of breaking the Pb-I bond is a process that mainly depends on interaction between the laser and the bulk, the height may not be enough to start the process in some cases.

### 7.2.2 Oscillating Intensity

As the intensities of the different surviving structures were investigated, a newly discovered and not yet understood phenomena of perovskites was observed - an oscillating intensity. If luminescence from all areas in the bulk appeared to follow the oscillation it would most likely be a result of experimental artifacts, such as variations in laser intensity.

By looking at the plotted intensity curve in 5.6 (c) it seems like the intensity of the bulk does not oscillate. Also, the oscillating intensity curves from the two different crystals seems to be slightly out of phase. It is possible that the phase difference comes from a, not yet explained, sample property or even from the atmosphere affecting the structures in various ways. Further investigation of which phenomena that causes the behavior is proceeding in the SMS group at Lund University Chemical Physics Department, where the work in this thesis contributes by relating the structural properties to the observed PL phenomena.

### 7.2.3 Blinking Causing Change of Emissive Point

Blinking "on" and "off" was connected to a "jump" (approximately 100 nm) for the average position of the Gaussian fitted to the emission profile from a crystal (Figure 5.7). This indicates that blinking happens as one part of the crystal completely quenches and stops emitting light. This can be explained by the theory of traps states lifetimes presented in Chapter 2.

In general, the radiative recombination in perovskites happens between an electron and hole band-to-band transition resulting in an emitted photon[10]. In an excited state this is the preferable radiative recombination process for all electrons. However, traps will still be present in the crystal and an evidence of that are the different PL lifetimes measured for different



crystals. A sudden drop in intensity together with a significant reduction in PL lifetime suggests that a localized trap with an average lifetime  $\tau_{trap}$  has been activated (possibly by photoexcitation). The activated trap cause electrons and holes in its surrounding to efficiently recombine non-radiative, causing a drastic drop in luminescent intensity.

Localized efficient traps causing drastic intensity drops can be explained analogously to a classical power failure in a city. If everything is working properly, all homes are supplied with electricity to use reading lamps and to stream movies on their laptops. Imagine only the reading lamp shutting down, as a movie on your laptop continues to play. In order to be able to read again you would exchange the lamp and again, everything is in order! However if both the lamp and the laptop shuts down, along with the streetlights outside at the same time as you hear the neighbor cursing out the window, there is by all evidences a system error somewhere where the electricity is connected. To adjust for this error some electrician would have to repair the generator of your neighborhood to again make all devices work again.

Connecting the blinking phenomena to the power failure in a neighbourhood, means that an activated efficient trap works in the same way as the generator. When the trap is activated (generator broken) all electrons and holes in a vast vicinity of the trap are efficiently recombined non-radiatively.

The blinking phenomena of perovskites are not yet understand but the results provided in my thesis works supports the explanation of an activated efficient trap.

### 7.3 Luminescent Life-Time of Different Structures

Measurements of the luminescent lifetimes for different MAPbI<sub>3</sub> structures, revealed a broad inhomogeneity throughout the experiments. Comparing the general outcome of the two synthesising methods it was concluded that with M2 a higher fraction of long luminescent lifetime structures are produced, while the clusters from the low concentration M1 samples did not show lifetimes above 25 ns. By observing the samples in the SEM it was possible to conclude some structural dependence of the lifetime.

The results showed that a more even crystal surface is associated with longer luminescent lifetimes, whereas an uneven surface shortens the lifetime drastically. It is therefore suggested that surface trap states serving as non-radiative recombination centers for charge carriers in MAPbI<sub>3</sub> has a large impact on the photophysical properties of the sample. Semiconductor surfaces and interfaces often contain a large number of recombination centers because of their termination of the semiconductor crystal, which leaves a large number of electrically active states, [20]. In addition, the surfaces and interfaces are more likely to contain impurities since they are exposed during the sample preparation process.

Comparing the structures from the bigger clusters from M1 the surface showed to have a similar, very "cracked" and inhomogeneous structure. The similarity reflects in the small variation of measured lifetimes reaching a maximum length of approximately 25 ns. For the varying crystal structures from M2 the lifetimes also showed a broad variation with maximum lifetimes of almost 200 ns for the most even structures.

Another result that also suggests the presence of more traps in an inhomogeneous surface is the difference in decay profiles. The long lifetime structure has a more monoexponential decay, while the shorter lifetime decays are fitted to be biexponential. This reveals different radiative recombination processes for the "on" and "off" stages of perovskites. This theory could further be investigated in experiments dependent of varying excitation power.

Since the carriers lifetime in perovskites have long diffusion lengths, excited electron and holes from the bulk can easily travel through the crystal surface to be trapped. Thus in this case the wanted long-diffusion-length property for use in solar cells serves negatively since traps will always be present. Our results are therefore highlighting the importance of an even structure for perovskite films in solar cell devices and our method allows us to study the structure dependent PL properties with a resolution down to approximately 10 nm.

### 7.3.1 Blinking and Lifetime

Analyzing the data from the lifetime recording for a series of frames it was concluded that the blinking process changes the luminescent lifetime. The average lifetime of the low and high level of intensity showed that the off-state was connected to a shortening in luminescent lifetime. This supports the theory of a local momentary activated non-radiative trap mentioned as candidate for the explanation of shift in localization for blinking objects Gaussian intensity maximum.

A sequentially activated non-radiative trap could also be an explanation to why blinking puts the degradation on hold [1]. If no long lived charge carriers are present in the conduction and valance band the local field gradient explained to induce ion migration may not be strong enough.

In the theory it was mentioned that one of the energies included as charge carriers are trapped is that related to the lattice relaxation in the vicinity of the trap origin. The rearrangement of the crystal lattice depending of whether a charge is trapped or not should by all means affect the duration of the "on" and "off" stages in intensity.

## Chapter 8

# Conclusion and future directions

During the last couple of years perovskite materials have shown to offer a lot of intriguing properties for the use in solar cell devices. Due to the high quantum yield, long diffusion length and broad absorption band, the efficiency of perovskite solar cells have increased from the first produced device in 2009 of 3.8 % [9] to reaching 22.1 % in early 2016 [11], making them a shooting star in the development of solar energy conversion.

To be able to in a larger extent use perovskite in various future technology devices some obstacles, including instability and toxicity, must be overcome. The interest and search for solutions to the perovskite problems has made the research field expand in the the last couple of years.

By studying the photoinduced degradation of perovskites in air, the results in my master thesis project connected a more defected surface structure to a degraded area in comparison to an undegraded area. These results contributed to the conclusion that transformation of MAPBI<sub>3</sub> into PbI<sub>2</sub> originated from the process of ion migration through the crystal due to a local field gradient induced by the photoexcitons (published in [1]).

The lifetime measurements resulted in a large inhomogeneity for different structures. Comparing the lifetime between some structures we found that a long charge carrier lifetime was associated with a more evenly crystalline structure with a monoexponential decay curve. The shorter lifetime of more inhomogeneous structures was suggested to depend partly on a higher concentration of structural non-radiative traps.

In connection to production of future solar cell devices it is very important to avoid traps in the largest possible extent. Through our measurements, structural surface traps seems to be a big obstacle in order to obtain the wanted properties of long charge carrier lifetime. As non-radiative traps are present, the long diffusion length serves negatively since it is easy for charges to travel to the trap state and the brightness drops. It has recently been reported that by chemical treatment of perovskites it is possible to greatly improve the brightness [7].

Another instability problem with perovskites is the sudden quenching of luminescence. In the results of my thesis the quenching was proved to be connected to a change in average position of the emission profile as well as a shortening of the luminescent lifetime. The average position change is not necessary depending on the shape of the crystal but it is a proof of some part of the crystal suddenly stops emitting light. These results supports the fact that blinking occurs from activation and deactivation of localized trap state,

somehow activated and deactivated causing efficient traps, which makes excited charge carriers in its surrounding to recombine non-radiatively.

Now, for future production of perovskite high power films in solar cell devices the importance of minimizing surface traps must be greatly considered. Along with a more homogeneous surface there may also be chemical treatments that could reduce the performance-limiting structures.

## Appendix A

# Equi-molar MAIPbI<sub>3</sub> Perovskite Preparation Instruction

### A.1 M1

#### A.1.1 PbI<sub>2</sub> + MAI (461 mg + 159 mg, 1:1 molar ratio) to prepare 0.8 M solution of MAPbI<sub>3</sub>

1. Weigh the components each of them in a vial. Weigh PbI<sub>2</sub> first. *It is OK to have excess of MA compound, but it is NOT good to have more Pb than needed.*
2. Add 1.25 ml of DMF and stir it on a hot plate (60 °C) for 8 h.

### A.2 M2

#### A.2.1 MAPbI<sub>3</sub> nano-wire preparation

1. Take 100 mg of PbAc<sub>2</sub> in a vial and add 1 ml of miliQ water, dissolve it properly by ultra-sonication at room temperature.
2. Take a clean (UV treated) glass slide (1 cm × 1 cm) and drop 10 μl of PbAc<sub>2</sub> solution (mass loading 1 mg/cm<sup>2</sup>). *The glass should be hydrophilic.*
3. Bake it for 30 min at 60 °C, take out the sample and cool it to room temperature. *The surface will be covered by PbAc<sub>2</sub> crystals.*
4. Prepare MAI solution in isopropanol (IPA), take 40 mg of MAI in a vial, add 1 ml of IPA and sonicate for 5 min, it will dissolve properly.
5. Take 1 ml of MAI solution in a vial, place PbAc<sub>2</sub> coated glass slide facing up in the vial for 20 h at room temperature, keep it in a dark place. *The surface become black already after 5-10 min, 20h is just to make the reaction as complete as possible.*
6. **Cleaning:** Take the glass slide out and dip it gently into another vial of IPA to remove residual salt. *Do not shake, crystals may fall of.*
7. Dry the film slowly under N<sub>2</sub> flow.



## References

- [1] Yuxi Tian Elin Källman Alexander Dobrovolsky Aboma Merdasa Monojit Bag and Ivan G. Scheblykin. "Super-Resolution Luminescence Microspectroscopy Reveals the Mechanism of Photoinduced Degradation in  $\text{CH}_3\text{NH}_3\text{PbI}_3$  Perovskite Nanocrystals". In: *The Journal of Physical Chemistry C* 69 (2016). URL: <http://dx.doi.org/10.1021/acs.jpcc.6b03512>.
- [2] Qimin Yan Audrius Alkauskas and Chris G. Van de Walle. "First-principles theory of nonradiative carrier capture via multiphonon emission". In: (2014). URL: <https://arxiv.org/pdf/1407.4197.pdf>.
- [3] Magdalena Lidia Ciurea. *Atomic Scale Design Network (ASDN) Trapping Phenomena in Nanocrystalline Semiconductors*. <http://asdn.net/asdn/physics/traps.php>. Accessed: 2016-05-20.
- [4] Qingfeng Dong et al. "Electron-hole diffusion lengths > 175 nm in solution-grown  $\text{CH}_3\text{NH}_3\text{PbI}_3$  single crystals". In: 347.6225 (2015), pp. 967–970. DOI: [10.1126/science.aaa5760](https://doi.org/10.1126/science.aaa5760).
- [5] S. Pathak L. E. Klintberg D. Jarausch R. Higler T. Leijtens S. D. Stranks H. J. Snaith R. T. Phillips et al. F. Deschler M. Price. "High Photoluminescence Efficiency and Optically Pumped Lasing in Solution-Processed Mixed Halide Perovskite Semiconductors." In: 5 (2014), pp. 1421–1426.
- [6] Steinbrück Sykora Hollingsworth Klimov Galland Ghosh and Htoon. "Two Types of Luminescence Blinking Revealed by Spectroelectrochemistry of Single Quantum Dots." In: 479 (2011), pp. 203–207.
- [7] Ansuman Halder et al. "Pseudohalide ( $\text{SCN}^-$ )-Doped  $\text{MAPbI}_3$  Perovskites: A Few Surprises". In: *The Journal of Physical Chemistry Letters* 6.17 (2015). PMID: 26291471, pp. 3483–3489. DOI: [10.1021/acs.jpcllett.5b01327](https://doi.org/10.1021/acs.jpcllett.5b01327). eprint: <http://dx.doi.org/10.1021/acs.jpcllett.5b01327>. URL: <http://dx.doi.org/10.1021/acs.jpcllett.5b01327>.
- [8] Mitch Jacoby. *The Future of Low-Cost Solar Cells*. <http://cen.acs.org/articles/94/i18/future-low-cost-solar-cells.html>. Accessed: 2016-06-07.
- [9] Akihiro Kojima et al. "Organometal Halide Perovskites as Visible-Light Sensitizers for Photovoltaic Cells". In: *Journal of the American Chemical Society* 131.17 (2009). PMID: 19366264, pp. 6050–6051. DOI: [10.1021/ja809598r](https://doi.org/10.1021/ja809598r). eprint: <http://dx.doi.org/10.1021/ja809598r>. URL: <http://dx.doi.org/10.1021/ja809598r>.

- [10] Rounak Naphade et al. "Hybrid Perovskite Quantum Nanostructures Synthesized by Electrospray Antisolvent–Solvent Extraction and Intercalation". In: *ACS Applied Materials & Interfaces* 8.1 (2016). PMID: 26690942, pp. 854–861. DOI: 10.1021/acsami.5b10208. eprint: <http://dx.doi.org/10.1021/acsami.5b10208>. URL: <http://dx.doi.org/10.1021/acsami.5b10208>.
- [11] *NREL Best Research Cell Efficiencies*. [http://www.nrel.gov/ncpv/images/efficiency\\_chart.jpg](http://www.nrel.gov/ncpv/images/efficiency_chart.jpg). Accessed: 2016-05-26.
- [12] *Ossila Perovskites and Perovskite Solar Cells: An Introduction*. <http://www.ossila.com/pages/perovskites-and-perovskite-solar-cells-an-introduction>. Accessed: 2016-05-26.
- [13] Dane W. de Quilettes et al. "Impact of microstructure on local carrier lifetime in perovskite solar cells". In: *Science* 348.6235 (2015), pp. 683–686. ISSN: 0036-8075. DOI: 10.1126/science.aaa5333. eprint: <http://science.sciencemag.org/content/348/6235/683.full.pdf>. URL: <http://science.sciencemag.org/content/348/6235/683>.
- [14] Negar Ashari Astani Basile F.E. Curchod Michael Graetzel Ursula Roethlisberger Simone Meloni Giulia Palermo. "Valence and conduction bands engineering in halide perovskites for solar cell applications". In: (2014). URL: <https://arxiv.org/ftp/arxiv/papers/1412/1412.3659.pdf>.
- [15] Dandan Song et al. "Managing Carrier Lifetime and Doping Property of Lead Halide Perovskite by Postannealing Processes for Highly Efficient Perovskite Solar Cells". In: *The Journal of Physical Chemistry C* 119.40 (2015), pp. 22812–22819. DOI: 10.1021/acs.jpcc.5b06859. eprint: <http://dx.doi.org/10.1021/acs.jpcc.5b06859>. URL: <http://dx.doi.org/10.1021/acs.jpcc.5b06859>.
- [16] Zhaoning Song et al. "Impact of Processing Temperature and Composition on the Formation of Methylammonium Lead Iodide Perovskites". In: *Chemistry of Materials* 27.13 (2015), pp. 4612–4619. DOI: 10.1021/acs.chemmater.5b01017. eprint: <http://dx.doi.org/10.1021/acs.chemmater.5b01017>. URL: <http://dx.doi.org/10.1021/acs.chemmater.5b01017>.
- [17] Yuxi Tian et al. "Enhanced Organo-Metal Halide Perovskite Photoluminescence from Nanosized Defect-Free Crystallites and Emitting Sites". In: *The Journal of Physical Chemistry Letters* 6.20 (2015). PMID: 26722793, pp. 4171–4177. DOI: 10.1021/acs.jpcllett.5b02033. eprint: <http://dx.doi.org/10.1021/acs.jpcllett.5b02033>. URL: <http://dx.doi.org/10.1021/acs.jpcllett.5b02033>.
- [18] Michael Wahl. *PicoQuant Time-Correlated Single Photon Counting*. [https://www.picoquant.com/images/uploads/page/files/7253/technote\\_tcspc.pdf](https://www.picoquant.com/images/uploads/page/files/7253/technote_tcspc.pdf). Accessed: 2016-05-24.
- [19] Yongbo Yuan and Jinsong Huang. "Ion Migration in Organometal Trihalide Perovskite and Its Impact on Photovoltaic Efficiency and Stability". In: *Accounts of Chemical Research* 49.2 (2016). PMID: 26820627, pp. 286–293. DOI: 10.1021/acs.accounts.5b00420. eprint:



<http://dx.doi.org/10.1021/acs.accounts.5b00420>.  
URL: <http://dx.doi.org/10.1021/acs.accounts.5b00420>.

- [20] B. Van Zeghbroeck. *Semiconductor Fundamentals Carrier recombination and generation*. [http://ecee.colorado.edu/~bart/book/book/chapter2/ch2\\_8.htm](http://ecee.colorado.edu/~bart/book/book/chapter2/ch2_8.htm). Accessed: 2016-05-30.